RSC Advances

PAPER

View Article Online
View Journal | View Issue

Cite this: *RSC Adv.*, 2021, **11**, 160

Design, synthesis and application in biological imaging of a novel red fluorescent dye based on a rhodanine derivative†

Zijing Li,[a] Bin Huang,[*b] Yuan Wang,[c] Wenbo Yuan,[a] Yijing Wu,[a] Ruitao Yu,[a] Guichuan Xing,[*d] Taotao Zou[*c] and Youtian Tao[*a]

Received 22nd October 2020
Accepted 10th December 2020

DOI: 10.1039/d0ra08998b

rsc.li/rsc-advances

A novel acceptor–donor–acceptor type molecule, namely 2-triphenylamine-1,3-dia[2-(3-ethyl-4-oxo-thiazolidin-2-ylidene)-malononitrile] (2RDNTPA), is designed and synthesized. 2RDNTPA exhibits a large Stokes shift of 244 nm and red fluorescence emission of 629 nm with a decent photoluminescence quantum yield of 13%. Furthermore, as a potential red fluorescent dye, 2RDNTPA can be applied in fluorescence imaging of living cancer cells (HepG2) with negligible cytotoxicity and a half maximal inhibitory concentration much more than 100 μM.

In recent years, imaging technology has achieved remarkable development, which can convert chemical and biological information into monitorable signals, making it possible to visually monitor different biological components and various physiological processes in living organisms.[1] Among various imaging technologies, fluorescence imaging has been considered as a promising technology for elucidating biological functions.[1–7] The usually utilized fluorescent dyes for fluorescence imaging are molecules with emission wavelength beyond 600 nm that allow for slight photo-damage on samples and low levels of auto fluorescence from biomolecules.[2,3] It is widely reported that heavy-metal complexes[8–10] and organic dyes are candidates for achieving red emission of fluorescence imaging. However, most heavy-metal complexes possess some drawbacks such as high cost, serious pollution and strong toxicity, which limit their applications.[8–10] Therefore, the development of fluorescent dyes with metal-free small organic dyes for efficient fluorescence imaging attracted more and more attention.

In general, the core properties of an efficient dye for fluorescence imaging include the following: (1) a large Stokes shift between excitation and emission;[3] (2) high photo-luminescence quantum yield (PLQY); (3) red or infrared emission to eliminate the backgrounds from biological environments; (4) good biocompatibility and low toxicity; (5) easy to synthesize. To date, some red or infrared light-emitting fluorophores such as Cy7-1,[2] AHGa,[4] DCF-MPYM,[5] *et al.* showed great potentials in fluorescence imaging. However, compared with conventional fluorescence dyes, fluorophores for efficient fluorescence imaging are still limited in number. It remains a challenge to develop brand-new fluorescent dyes for fluorescence imaging.

Rhodanine,[23–25] a five-membered S,N-heterocycle, can serve as a building block for organic dyes in biomedical fields such as biomolecule fluorescent labeling,[11] proteomics,[12] photodynamic therapy,[13–15] live cell imaging,[16–19] antitumor drugs,[20] DNA detection,[8] pH probes,[21] fluorescent sensors,[22] *etc.* Owning to their strong electron-withdrawing properties, rhodanine derivatives have been broadly utilized as acceptors for the design of donor–acceptor (D–A) type photovoltaic materials in organic solar cells (OSCs).[39] However, up to now, there is no report on D–A type dyes based on rhodanine derivatives with efficient red emission for fluorescence imaging.

Herein, we designed and synthesized a new acceptor–donor–acceptor (A–D–A) type molecule 2-triphenylamine-1,3-dia[2-(3-ethyl-4-oxo-thiazolidin-2-ylidene)-malononitrile] (2RDNTPA, Scheme 1), in which triphenylamine (TPA) and rhodanine derivative of 2-(3-ethyl-4-oxo-thiazolidin-2-ylidene)-malononitrile (RDN) act as the electron donor and acceptor group, respectively. TPA unit is widely used as electron donor in emitters for its suitable steric hindrance and strong electron-donating ability,[26,27] while RDN unit with two cyan groups possesses strong electron-accepting ability and high molecular rigidity. 2RDNTPA exhibits a large Stokes shift of 244 nm and red fluorescence emission of 629 nm with a decent PLQY of 13%. More importantly, it is demonstrated that 2RDNTPA can

[a]*Key Laboratory of Flexible Electronics, Institute of Advanced Materials, Nanjing Tech University, Nanjing, P. R. China. E-mail: iamyttao@njtech.edu.cn*

[b]*College of Life Sciences and Chemistry, Jiangsu Key Laboratory of Biofunctional Molecule, Jiangsu Second Normal University, Nanjing, P. R. China. E-mail: huangbinhb31@sina.com*

[c]*Guangdong Key Laboratory of Chiral Molecule and Drug Discovery, School of Pharmaceutical Sciences, Sun Yat-Sen University, Guangzhou, P. R. China. E-mail: zoutt3@mail.sysu.edu.cn*

[d]*Institute of Applied Physics and Materials Engineering, University of Macau, Macao SAR 999078, China. E-mail: gcxing@um.edu.mo*

† Electronic supplementary information (ESI) available. See DOI: 10.1039/d0ra08998b

be applied in fluorescence imaging of the living cancer cells (HepG2) with negligible cytotoxicity.

Synthetic routes of 2RDNTPA were shown in Scheme 1 and the detailed procedure can be found in the ESI.† First, the key intermediate 2-triphenylaminebenzene-1,3-dialdehyde (2AIDTPA) was prepared by Suzuki coupling reaction between 2-bromobenzene-1,3-dialdehyde and *N*,*N*-diphenyl-4-(4,4,5,5-tetramethyl-1,3,2-dioxaborolan-2-yl)aniline. Then 2AIDTPA was converted to 2RDNTPA *via* Knoevenagel condensation[30] with 2-(3-ethyl-4-oxo-thiazolidin-2-ylidene)-malononitrile. The intermediate and target compound were fully identified by ^{1}H NMR (Fig. S1 and S2, ESI†), MS (Fig. S3, ESI†) and elemental analysis. Due to the substituent effects on the double bonds between RDN groups and the central benzene cycle, 2RDNTPA may have three kinds of *cis–trans* isomers (*e.g.*: EE, ZZ and EZ). In general, *E*-isomer is more stable than the corresponding *Z*-isomer. In addition, the ^{1}H NMR of two RDN groups are the same (Fig. S2†), indicating that 2RDNTPA possesses a symmetrical structure. As a result, we can conclude that the reported structure of 2RDNTPA belongs to an EE isomer (Scheme 1).

Thermal gravimetric analysis showed the decomposition temperature was about 369 °C with 5% loss of weight (Fig. S4, ESI†), while the glass transition temperature was not found during the second heating of differential scanning calorimetry measurement. The thermal analysis results clearly demonstrated the favorable thermal stability of 2RDNTPA for biological imaging.

To predict the electronic distribution of 2RDNTPA, density functional theory (DFT) calculations were performed. As shown in Fig. 1a, 2RDNTPA displayed a highly twisted molecular structure with large torsion angles of 60° and 30° between RDN units and the central phenyl unit. As expected, the highest occupied molecular orbital (HOMO) and the lowest unoccupied molecular orbital (LUMO) of 2RDNTPA were located on the donor and acceptor unit, respectively.[33] The HOMO and LUMO energy levels of 2RDNTPA were estimated to be −5.27 and −2.95 eV, respectively (Fig. 1b). Accordingly, the optical bandgap (E_g) of 2RDNTPA was calculated to be 2.32 eV.

The photophysical properties of 2RDNTPA in powder were investigated. From the UV-vis absorption spectra (Fig. 2a), the absorption peak at 298 nm can be attributed to the intense absorption from TPA centered n–π* transition, while the broad absorption band in the range of 350–500 nm with peak at 385 nm originate from intramolecular charge transfer transition (ICT).[33–38] From the onset of the absorption spectra, E_g of 2RDNTPA was calculated to be 2.25 eV, which agrees well with the theoretical result. As shown in Fig. 2a, 2RDNTPA exhibited

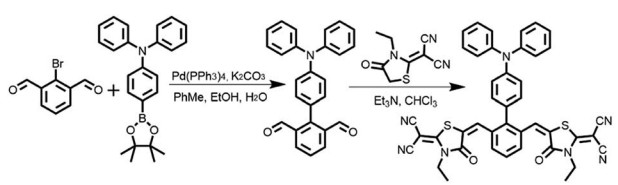

Scheme 1 Synthetic route of 2RDNTPA.

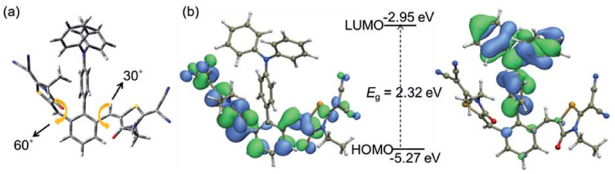

Fig. 1 (a) Molecular structure, (b) HOMO (left) and LUMO (right) distributions, and theoretically calculated HOMO, LUMO of 2RDNTPA.

an obviously red emission peak at 629 nm with PLQY of 13% (Fig. S5†). The Stokes shift of 2RDNTPA between excitation (385 nm) and emission (629 nm) was calculated to be 244 nm, which may facilitate the elimination of background interference effectively. From the fluorescence and phosphorescence spectra of 2RDNTPA at 77 K (Fig. 2b), the singlet energy level and triplet energy level of 2RDNTPA were estimated to be 2.25 and 1.99 eV, respectively. The transient PL decay curve of 2RDNTPA was also depicted in Fig. 2c, which exhibited two components decay with an average lifetime of 9.26 ns.

We also measured UV-vis and fluorescence spectra of 2RDNTPA in different solvents. As shown in Fig. S6 and Table S1,† polarity of the solvents has negligible influence on the UV-vis spectra of 2RDNTPA. In contrast, the emission spectra of 2RDNTPA is gradually red-shifted with increasing solvent polarity, indicating typical ICT feature (Fig. S7 and Table S1†). To explore the aggregated luminescence properties, the PL intensity of 2RDNTPA in the mixture of chloroform and methanol with various methanol ratio fractions was measured. As shown in Fig. S8,† the PL intensity showed an overall slow decline when methanol fractions (f_w) increased from 0% to 90%, showing obvious aggregation-caused quenching properties of 2RDNTPA in the chloroform/methanol system. To evaluate the light stability of 2RDNTPA, the absorption intensity in dimethyl sulfoxide solution with various irradiation times of 365 nm ultraviolet lamp was characterized. The absorption intensity showed slow decline when irradiation time increased from 0 to 24 h (Fig. S9†). It was evident that 2RDNTPA proved to be highly photo-stable.

The electrochemical properties of 2RDNTPA were investigated by cyclic voltammetry (CV) measurements. As depicted in Fig. S10,† 2RDNTPA displayed quasi-reversible oxidation process assigned to the triphenylamine units.[36,37]

Based on the onset of oxidation from CV curve, the HOMO energy level was estimated to be −5.29 eV. From the equation

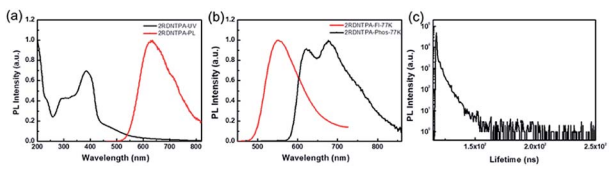

Fig. 2 (a) Normalized UV-vis absorption and PL spectra (excitation of 385 nm) of compound 2RDNTPA in powder. (b) Normalized fluorescence (Fl) and phosphorescence (Phos) spectra with 0.1 s delay of compound 2RDNTPA in powder at 77 K. (c) Transient decay curves of compound 2RDNTPA in powder.

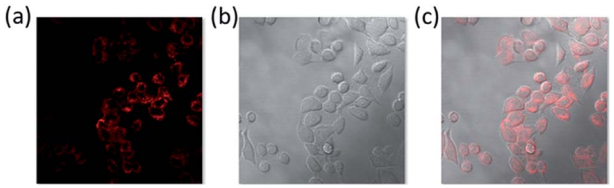

Fig. 3 (a) CLSM (excitation of 407 nm and emission of 620 nm) images of 2RDNTPA in living HepG2 cell (10 μM incubation overnight). (b) Bright field. (c) Merged image.

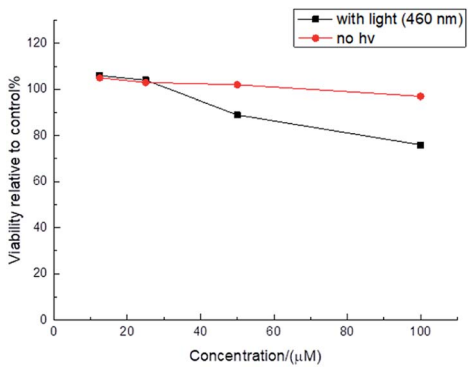

Fig. 4 Cell toxicity assay of 2RDNTPA in living HepG2 cell.

$E_{LUMO} = E_{HOMO} + E_g$, here the E_g value was estimated from the edge of UV-vis absorption, the LUMO energy level was estimated to be −3.04 eV, which are in accordance with the calculated results.

The unique photophysical properties of 2RDNTPA led us to investigate its application in biological imaging. We treated living HepG2 liver cancer cells with 2RDNTPA solution. The detailed procedure can be found in the ESI.† Then confocal laser scanning microscopy (CLSM) imaging was carried out by utilizing the red emission of 2RDNTPA to investigate the cellular uptake and sub-organelle localization in cancer cells.[31,32] As shown in Fig. 3, CLSM imaging can clearly characterize the situation inside the cell with strong red fluorescence close to 620 nm, which agrees well with the excellent red light-emitting performance of 2RDNTPA. It is worth noting that the cells did not show obvious morphology change, indicating good biocompatibility of 2RDNTPA in living HepG2 cell. As we all know, the low cytotoxicity of organic dyes is a key criterion for live cell imaging.[1] So we conducted 2RDNTPA *in vitro* cytotoxicity experiments.[28,29] As shown in Fig. 4, when the concentration of 2RDNTPA reach to 100 μM, more than 95% cells still survive at no *hv* environment. According to U.S. National Cancer Institute recommends,[40] IC_{50} (inhibitory concentrations) greater than 50 μM can be considered as invalid during cell toxicity assay. The results suggest that 2RDNTPA shows negligible toxicity in living HepG2 liver cancer cells whether under illuminated conditions or not. The good biocompatibility and low cytotoxicity of 2RDNTPA indicate that it can be utilized as an efficient dye for live cell imaging to replace traditional heavy-metal complexes with high cytotoxicity.[41]

In summary, we have developed an A–D–A structured red fluorescent dye 2RDNTPA, in which TPA and rhodanine derivative RDN act as the electron donor and acceptor group, respectively. Based on theoretical calculations, photophysical and electrochemical tests, the photophysical properties of 2RDNTPA have been systematically investigated. 2RDNTPA exhibits a large Stokes shift of 244 nm and red fluorescence emission of 629 nm with a decent photoluminescence quantum yield of 13%. By using 2RDNTPA as a red dye in biological imaging of the living HepG2 cancer cells, we have obtained commendable imaging results with IC_{50} of much more than 100 μM. The present work provides a new strategy for the design and application of organic fluorescent dyes.

Conflicts of interest

There are no conflicts to declare.

Acknowledgements

We thank National Natural Science Foundation of China (No. 51103023, 91833304 and 61761136013), NSF of Jiangsu Province (No. XYDXX-026) and the Natural Science Foundation of the Jiangsu Higher Education Institutions (No. 19KJB150006). G. C. X. acknowledges the Science and Technology Development Fund, Macao SAR (File no. FDCT-0044/2020/A1, FDCT-091/2017/A2, FDCT-014/2017/AMJ), UM's research fund (File no. MYRG2018-00148-IAPME), the Natural Science Foundation of China (91733302, 61935017), Natural Science Foundation of Guangdong Province, China (2019A1515012186).

Notes and references

1 Y. Yang, Q. Zhao, W. Feng and F. Li, *Chem. Rev.*, 2013, **113**, 192–270.
2 Y. Li, Y. Sun, J. Li, Q. Su, W. Yuan, Y. Dai, C. Han, Q. Wang, W. Feng and F. Li, *J. Am. Chem. Soc.*, 2015, **137**, 6407–6416.
3 S. Zhang, J. Fan, Z. Li, N. Hao, J. Cao, T. Wu, J. Wang and X. Peng, *J. Mater. Chem. B*, 2014, **2**, 2688–2693.
4 B. Lozano-Torres, I. Galiana, M. Rovira, E. Garrido, S. Chaib, A. Bernardos, D. Muñoz-Espín, M. Serrano, R. Martínez-Máñez and F. Sancenón, *J. Am. Chem. Soc.*, 2017, **139**, 8808–8811.
5 X. Xiong, F. Song, J. Wang, Y. Zhang, Y. Xue, L. Sun, N. Jiang, P. Gao, L. Tian and X. Peng, *J. Am. Chem. Soc.*, 2014, **136**, 9590–9597.
6 T. Li, D. Yang, L. Zhai, S. Wang, B. Zhao, N. Fu, L. Wang, Y. Tao and W. Huang, *Adv. Sci.*, 2017, **4**, 1600166.
7 F. Ni, Z. Zhu, X. Tong, M. Xie, Q. Zhao, C. Zhong, Y. Zou and C. Yang, *Chem. Sci.*, 2018, **9**, 6150–6155.
8 M. R. Gill and J. A. Thomas, *Chem. Soc. Rev.*, 2012, **41**, 3179–3192.
9 K. Hanaoka, K. Kikuchi, S. Kobayashi and T. Nagano, *J. Am. Chem. Soc.*, 2007, **129**, 13502–13509.
10 A. Gorman, J. Killoran, C. O'Shea, T. Kenna, W. Gallagher and D. O'Shea, *J. Am. Chem. Soc.*, 2004, **126**, 10619–10631.

11 A. Toutchkine, V. Kraynov and K. Hahn, *J. Am. Chem. Soc.*, 2003, **125**, 4132–4145.
12 K. Janina, J. Katarzyna and O. Łukasz, *J. Mol. Struct.*, 2015, **1084**, 114–121.
13 P. Nowaksliwinska, A. Karocki, M. Elas, A. Pawlak, G. Stochel and K. Urbanska, *Biochem. Biophys. Res. Commun.*, 2006, **349**, 549–555.
14 D. L. Traul and F. Sieber, *J. Photochem. Photobiol., B*, 2015, **153**, 153–163.
15 G. S. Anderson, K. Miyagi, R. W. Sampson and F. Sieber, *J. Photochem. Photobiol., B*, 2002, **68**, 101–108.
16 X. Zhang, Z. Gu, L. Liu, S. Wang and G. Xing, *Chem. Commun.*, 2015, **51**, 8606–8609.
17 A. Nahain, J. E. Lee, J. H. Jeong and S. Y. Park, *Biomacromolecules*, 2013, **14**, 4082–4090.
18 H. H. Pham, C. Szentgyorgyi, W. L. Brotherton, B. F. Schmidt, K. J. Zanotti, A. S. Waggoner and B. A. Armitage, *Org. Biomol. Chem.*, 2015, **13**, 3699–3710.
19 E. E. Rastede, M. Tanha, D. Yaron, S. C. Watkins, A. S. Waggoner and B. A. Armitage, *Photochem. Photobiol.*, 2015, **14**, 1703–1712.
20 D. Kaminskyy, B. Bednarczykcwynar, O. Vasylenko, O. B. Kazakova, B. Zimenkovsky, L. Zaprutko and R. Lesyk, *Med. Chem. Res.*, 2012, **21**, 3568–3580.
21 L. He, W. Lin, Q. Xu and H. Wei, *ACS Appl. Mater. Interfaces*, 2014, **6**, 22326–22333.
22 K. Krumova and G. Cosa, *J. Am. Chem. Soc.*, 2010, **132**, 17560–17569.
23 H. Li, J. Yang, S. Ma and C. Qiao, *Bioorg. Med. Chem.*, 2012, **20**, 4194–4200.
24 W. Li, C. Zheng, L. Sun, M. Song, Y. Wu, Y. Li, Y. Liu and H. Piao, *Arch. Pharmacal Res.*, 2014, **37**, 852–861.
25 Y. Zhang, S. Wang, S. Wu, S. Zhu, G. Dong, Z. Miao, J. Yao, W. Zhang, C. Sheng and W. Wang, *ACS Comb. Sci.*, 2013, **15**, 298–308.
26 A. Mishra, M. Fischer and P. Bäuerle, *Angew. Chem., Int. Ed.*, 2009, **48**, 2474–2499.
27 Y. Shirota and H. Kageyama, *Chem. Rev.*, 2007, **107**, 953–1010.
28 K. Takasu, H. Inoue, H. Kim, M. Suzuki, T. Shishido, Y. Wataya and M. Ihara, *J. Med. Chem.*, 2002, **45**, 995–998.
29 K. Takasu, K. Pudhom, M. Kaiser, R. Brun and M. Ihara, *J. Med. Chem.*, 2006, **49**, 4795–4798.
30 G. Angajala, V. Aruna and R. Subashini, *J. Mol. Struct.*, 2021, **1224**, 129286.
31 J. Xiang, Y. Liu, D. Sun, S. Zhang, Y. Fu, X. Zhang and L. Wang, *Dyes Pigm.*, 2012, **93**, 1481–1487.
32 D. Gao, A. Li, L. Guan, X. Zhang and L. Wang, *Dyes Pigm.*, 2016, **129**, 163–173.
33 Y. Tao, K. Yuan, T. Chen, P. Xu, H. Li, R. Chen, C. Zheng, L. Zhang and W. Huang, *Adv. Mater.*, 2014, **26**, 7931–7958.
34 W. Zeng, T. Zhou, W. Ning, C. Zhong, J. He, S. Gong, G. Xie and C. Yang, *Adv. Mater.*, 2019, **31**, 1901404.
35 J. Chen, K. Wang, C. Zheng, M. Zhang, Y. Shi, S. Tao, H. Lin, W. Liu, W. Tao, X. Ou and X. Zhang, *Sci. Adv.*, 2018, **5**, 1800436.
36 W. Zeng, H. Lai, W. Lee, M. Jiao, Y. Shiu, C. Zhong, S. Gong, T. Zhou, G. Xie, M. Sarma, K. Wong, C. Wu and C. Yang, *Adv. Mater.*, 2017, **30**, 1704961.
37 F. Xie, H. Li, G. Dai, Y. Li, T. Cheng, M. Xie, J. Tang and X. Zhao, *ACS Appl. Mater. Interfaces*, 2019, **11**, 26144–26151.
38 Y. Luo, S. Li, Y. Zhao, C. Li, Z. Pang, Y. Huang, M. Yang, L. Zhou, X. Zheng, X. Pu and Z. Lu, *Adv. Mater.*, 2020, **32**, 2001248.
39 Q. Wei, W. Liu, M. Leclerc, J. Yuan, H. Chen and Y. Zou, *Sci. China: Chem.*, 2020, **63**, 1352–1366.
40 J. L. Sebaugh, *Pharm. Stat.*, 2011, **10**, 128–134.
41 L. Xian, F. Xu, J. Liu, N. Xu, H. Li, H. Ge, K. Shao, J. Fan, G. Xiao and X. Peng, *J. Am. Chem. Soc.*, 2019, **141**, 20490–20497.